ISSN 1070-3284, Russian Journal of Coordination Chemistry, 2016, Vol. 42, No. 6, pp. 378–384. © Pleiades Publishing, Ltd., 2016.

Anion-Assisted Two Group IIB Metallic Coordination Architecture and Luminescence Performance[1]

J. Y. Hu[a,*], C. L. Liao[b], C. C. Zhang[a], S. F. Chen[a], J. S. Zhang[a], and J. A. Zhao[a,*]

[a] *College of Chemical and Material Engineering, Henan University of Urban Construction, Pingdingshan, Henan, 467036 P.R. China*

[b] *College of Life Science and Engineering, Henan University of Urban Construction, Pingdingshan, Henan, 467036 P.R. China*

**e-mail: hujiyong@hncj.edu.cn; zjinan@zzu.edu.cn*

Received June 15, 2015

Abstract—React of cadmium salts with 4,4'-bis((2-(pyridin-2-yl)-1*H*-benzo[d]imidazol-1-yl)methyl)biphenyl (Bpbib) yields two one-dimensional (1D) coordination architectures of two new complexes—$\{[Cd_2(Bpbib)_2(NO_3)_4] \cdot CH_3OH\}_n$ (**I**) and $\{[Cd(Bpbib)Cl_2] \cdot 2CH_3OH\}_n$ (**II**). Complexes **I** and **II** were characterized by the elemental analyses, photoluminescence and emission spectra and single-crystal X-ray diffraction (CIF files CCDC nos. 1046021 (**I**), 1046022 (**II**)). Complex **I** is a helical array, whereas **II** features a zigzag pattern, depending upon the type of their associated anions. In addition to the primary organic linker, the counter anions also have a dominant influence on the overall structures, and even arouse the luminescence performance diversity.

DOI: 10.1134/S1070328416060026

INTRODUCTION

The observed performances are very much affected by subtle changes within the network structure of polymeric entities, which propels the development of synthetic strategies to afford the desired product with a predefined property [1–3]. Controllable synthesis is normally influenced by the organic linker geometry, solvent, anions, and coordination preference of metal centers, etc. Apart from those, the widely applied organic linker generally contains two or more functional moieties, which is a key factor for the structural assemblies [4, 5]. Among the organic building block, pyridin-2-yl-1H-benzimidazole moiety bears several coordinated sites, and the adjacent nitrogen atoms assist strong binding ability, which are further connected by biphenyl to aid the formation of a flexible organic linker. Based on such flexibility endowed by methylene together with biphenyl groups, the organic linker can adopt suitable conformation according to geometric needs of metal centers [6, 7].

Besides the organic linker, the anion effect is another key factor. The roles of anions, such as template effect, rich coordination tendency and hydrogen bonding interactions with receptors are crucial to enrich the structural diversity, especially for those with neutral multidentate organic linkers [8–12]. The variation of such character is usually considered for yielding functional molecular architecture. For example, Li group reported two anion-directed Hg(II) complexes, and the anion-controlled color changes depending on the anion feature, which may aid the understanding structure-color relationship [13–15]; Wang group reported the important effect of anions on the Ag(I) architectures [16]; Guo and his collaborator reported four structural diverse Cd(II) complexes regulated by distinct anions as well [17]. Thus, pyridin-benzimidazole-containing organic linker and the inorganic anion are complementary in their coordination preferences and may act synergetically to afford unique motifs with beautiful aesthetics and useful functional performances. To evaluate the anion role on the structural diversities and their behavioral alterations, the Cd salts with distinct anions were employed to react with neutral ligand for the construction of diverse complexes.

EXPERIMENTAL

Materials and general methods. All the starting materials were purchased commercially as reagent grade and used without further purification. 4,4'-Bis((2-(pyridin-2-yl)-1*H*-benzo[d]imidazol-1-yl)methyl)biphenyl (Bpbib) was synthesized according a literature method [18]. The thermogravimetric experiments were performed using a TGA/METTLER instrument heated from 35–900°C (heating rate at 10°C/min, air stream). The FT-IR spectra were recorded on a Nicolet IS10 spectrophotometer from KBr pellets in the region of 400–4000 cm^{-1}. Elemental analyses (C, H, and N) were carried out on a Flash EA 1112 elemental analyzer. The fluorescence

[1] The article is published in the original.

Table 1. Crystallographic data and structure refinement for complexes **I**, **II**

Parameter	Value	
	I	**II**
Fw	1642.21	816.05
Temperature, K	100.00(2)	100.01(10)
Crystal system	Monoclinic	Monoclinic
Space group	$P2_1/n$	$I2/c$
a, Å	10.3878(3)	13.1838(5)
b, Å	10.3881(3)	12.0050(4)
c, Å	32.2828(8)	22.9317(8)
β, deg	97.880(3)	106.187(4)
V, Å^3	3450.75(16)	3485.6(2)
Z	2	4
ρ_{calcd}, g cm^{-3}	1.567	1.555
μ, mm^{-1}	0.696	6.799
F(000)	1652.0	1664.0
Crystal size, mm^3	0.13 × 0.11 × 0.09	0.12 × 0.11 × 0.09
θ Range for data collection, deg	2.92–26.73	4.01–76.58
Index ranges *hlk*	$-13 \leqslant h \leqslant 12$ $-13 \leqslant k \leqslant 10$ $-40 \leqslant l \leqslant 40$	$-15 \leqslant h \leqslant 16$ $-14 \leqslant k \leqslant 10$ $-28 \leqslant l \leqslant 28$
Collected/independent reflections	22032/7290	7462/3590
R_{int}	0.0444	0.0337
Reflections with $I \geqslant 2\sigma(I)$	6281	3411
Goodness-of-fit on F^2	1.187	1.082
Final R_1, wR_2*	0.0860, 0.1802	0.0819, 0.2229
Largest diff. peak and hole, *e* Å^{-3}	1.92/–1.61	7.22/–2.03

* $R_1 = \Sigma||F_o| - |F_c||/\Sigma|F_o|$; $wR_2 = [\Sigma w(F_o^2 - F_c^2)^2/\Sigma w(F_o^2)^2]^{1/2}$.

measurements were performed with spectrofluorimeter Hitachi F-4600 at ambient temperature in solid state with the excitation slit width of 1 nm and emission slit width of 2.5 nm.

Synthesis of $\{[Cd_2(Bpbib)_2(NO_3)_4] \cdot CH_3OH\}_n$ (I). $Cd(NO_3)_2 \cdot 4H_2O$ (0.0046 g, 0.015 mmol) dissolved in methanol (1 mL) was added to a chloroform solution (1 mL) of Bpbib (0.0057 g, 0.01 mmol). The mixture was left to heat at 85°C for two days, and then the reaction system was cooled to room temperature causing the formation of block product in 64% yield (based on Cd).

For $C_{77}H_{60}N_{16}O_{13}Cd_2$

anal. calcd., %:	C, 56.32;	H, 3.68;	N, 13.65.
Found, %:	C, 56.12;	H, 3.60;	N, 13.74.

IR (KBr; ν, cm^{-1}): 3449 m, 3063 w, 2924 w, 1597 m, 1499 m, 1458 m, 1426 s, 1384 s, 1345 m, 1297 s, 1172 w, 1032 m, 1004 w, 821 m, 739 m.

Synthesis of $\{[Cd(Bpbib)Cl_2] \cdot 2CH_3OH\}_n$ (II). A chloroform solution (1 mL) of Bpbib (0.0057 g, 0.01 mmol) was added dropwise to a methanol (1 mL) solution of $Cd(ClO_4)_2 \cdot 6H_2O$ (0.0063 g, 0.015 mmol). The mixture was sealed in a glass reactor and heated at 85°C for two days, and then the reaction system was cooled to room temperature causing the formation of product. The resultant crystals were isolated and dried in air. The chloride anion may derive from the thermolysis of chloroform. The y ield was 30% (based on Cd).

For $C_{40}H_{36}N_6O_2Cl_2Cd$

anal. calcd., %:	C, 58.87;	H, 4.45;	N, 10.30.
Found, %:	C, 59.01;	H, 4.32;	N, 10.18.

IR (KBr; ν, cm^{-1}): 3436 m, 3054 w, 2922 w, 2854 w, 1640 m, 1590 m, 1478 m, 1421 s, 1329 m, 1159 w, 1122 w, 827 m, 757 s, 694 w.

Table 2. Selected bond lengths (Å) and angles (deg) for complexes **I**, **II***

Bond	*d*, Å	Bond	*d*, Å
		I	
Cd(1)–O(1)	2.435(5)	Cd(1)–N(5)$^{\#1}$	2.249(6)
Cd(1)–N(2)	2.299(6)	Cd(1)–O(3)	2.509(5)
Cd(1)–O(4)	2.441(6)	Cd(1)–N(1)	2.471(6)
Cd(1)–N(4)$^{\#1}$	2.612(7)		
		II	
Cd(1)–N(2)	2.381(5)	Cd(1)–N(1)	2.436(5)
Cd(1)–Cl(1)	2.489(5)		
Angle	ω, deg	Angle	ω, deg
		I	
O(1)Cd(1)O(4)	79.98(18)	O(1)Cd(1)O(3)	51.75(16)
O(1)Cd(1)N(4)$^{\#1}$	130.04(17)	O(1)Cd(1)N(1)	158.15(18)
N(5)$^{\#1}$Cd(1)N(2)	155.1(2)	N(5)$^{\#1}$Cd(1)O(1)	90.68(19)
N(5)$^{\#1}$Cd(1)O(4)	127.5(2)	N(5)$^{\#1}$Cd(1)O(3)	90.84(19)
N(5)$^{\#1}$Cd(1)N(4)$^{\#1}$	66.8(2)	N(5)$^{\#1}$Cd(1)N(1)	98.4(2)
N(2)Cd(1)O(3)	87.07(18)	N(2)Cd(1)O(1)	107.19(19)
N(2)Cd(1)N(1)	71.3(2)	N(2)Cd(1)O(4)	74.0(2)
		O(4)Cd(1)O(3)	119.81(17)
		II	
N(2)Cd(1)Cl(1)	99.35(14)	N(2)Cd(1)N(2)$^{\#1}$	162.3(2)
N(2)$^{\#1}$Cd(1)N(1)	97.08(16)	N(2)Cd(1)N(1)	68.40(16)
N(1)$^{\#1}$Cd(1)Cl(1)$^{\#1}$	92.0(2)	N(1)$^{\#1}$Cd(1)Cl(1)	153.0(2)
		Cl(1)Cd(1)Cl(1)$^{\#1}$	108.9(4)

* Symmetry transformation used to generate equivalent atoms: $^{\#1}$ $3/2 - x$, $1/2 + y$, $3/2 - z$ for **I**; $^{\#1}$ $1 - x$, y, $1/2 - z$ for **II**.

X-ray structure determination. A crystal suitable for X-ray determination was mounted on a glass fiber. The data was collected on a SuperNova with graphite monochromated radiation with graphite monochromated MoK_α (λ = 0.71073 Å) for **I** and CuK_α (λ = 1.54184 Å) for **II** at 100 K. The structures were solved by direct methods and refined by full-matrix least-squares. The non-hydrogen atoms were refined with anisotropic thermal parameters. All calculations were completed using the SHELXTL-97 program system [19–22]. Hydrogen atoms were assigned idealized positions and included in structure factor calculations. The final cycle of full-matrix least-squares refinement was based on the observed reflections and variable parameters. Table 1 gives the crystallographic crystal data and structure processing parameters, and the selected bond lengths and angles of them are listed in Table 2.

Supplementary material for structures has been deposited with the Cambridge Crystallographic Data Centre (nos. 1046021 (**I**), 1046022 (**II**); deposit@ccdc.cam.ac.uk or http://www.ccdc.cam.ac.uk).

RESULTS AND DISCUSSION

The asymmetric unit of **I** consists of one Cd(II) center, one Bpbib spacer, two nitrate anions and half a methanol moiety. The Cd(II) center is coordinated to four nitrate oxygen atoms and four nitrogen atoms (Fig. 1a). The Cd(1)···N(4) bonds length, 2.613 Å, is longer than normal Cd–N bonds but much shorter than the sum of the corresponding van der Waals radii (4.04 Å), indicating that weak interaction is present [23]. The long Cd–O distance, 2.667 Å, is also within the reported bond value [24]. The nature of the binding of these anions was unambiguous as defined by their Cd–O distances. Two bidentate NO_3^- anions are binding in terminal fashion. The eight-coordinated Cd(II) center affording a 1D helical chain, running along *y* axis, was linked by *cis* Bpbib (Fig. 2). The dihedral angles of pyridyl ring and benzimidazole moiety, benzene ring of biphenyl moiety are 39.466° and 25.419°, respectively. And the angle and twist angles around methylene equal to 111.687° and 36.079°, separately. In this case, each Bpbib is linked to two Cd(II) centers with two pyridin-2-yl-1*H*-benzimidazole

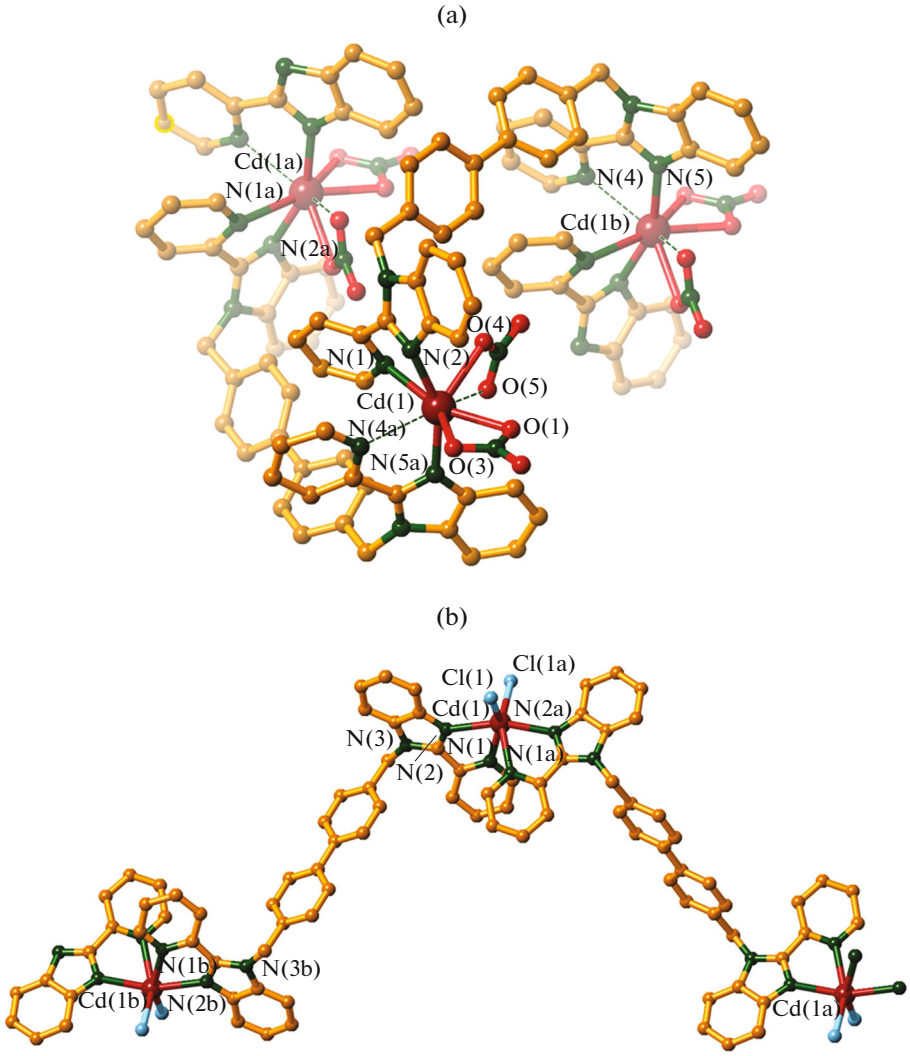

Fig. 1. Coordination environment of **I** (a) and **II** (b) with part atom numbering scheme.

moieties with the adjacent Cd···Cd separation of 11.505 Å. To compare the conformation manner, crystal structure of free Bpbib had been analysed as well (Fig. 3a). The *cis* free Bpbib has an inversion center locating on the center of C(17) and C(17a) bond, in which the dihedral angle of pyridyl ring and benzimidazole moiety is 17.245°. And the corresponding angle and twist angles around methylene are 112.805° and 133.129°, respectively.

The Bpbib acts as a tetradentate connector by linking two symmetric related units. The centroid separation between the imdazole and pyridyl is 3.569 Å with the dihedral angle of 4.8°, illustrating the presence of face to face π···π interactons, which extends the chains in *z* axis direction (Fig. 3b). The H(25)···Cg (adjacent benzimidazole ring) separation is 2.635 Å, which extends the adjacent chains in *x* axis direction (Fig. 3c). The C···O separations are 2.89(2) Å for C(39)···O(6), 3.112(16) Å for C(10)···O(7), 3.218(9) Å for C(26)···O(3), 3.276(9) Å for C(15)···O(4), which are within the reported values [25]. Apart from the

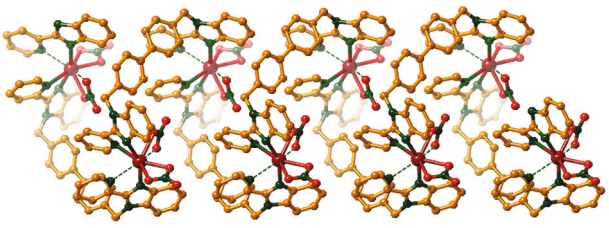

Fig. 2. The one-stranded helical chain motif of **I** running along *y* axis.

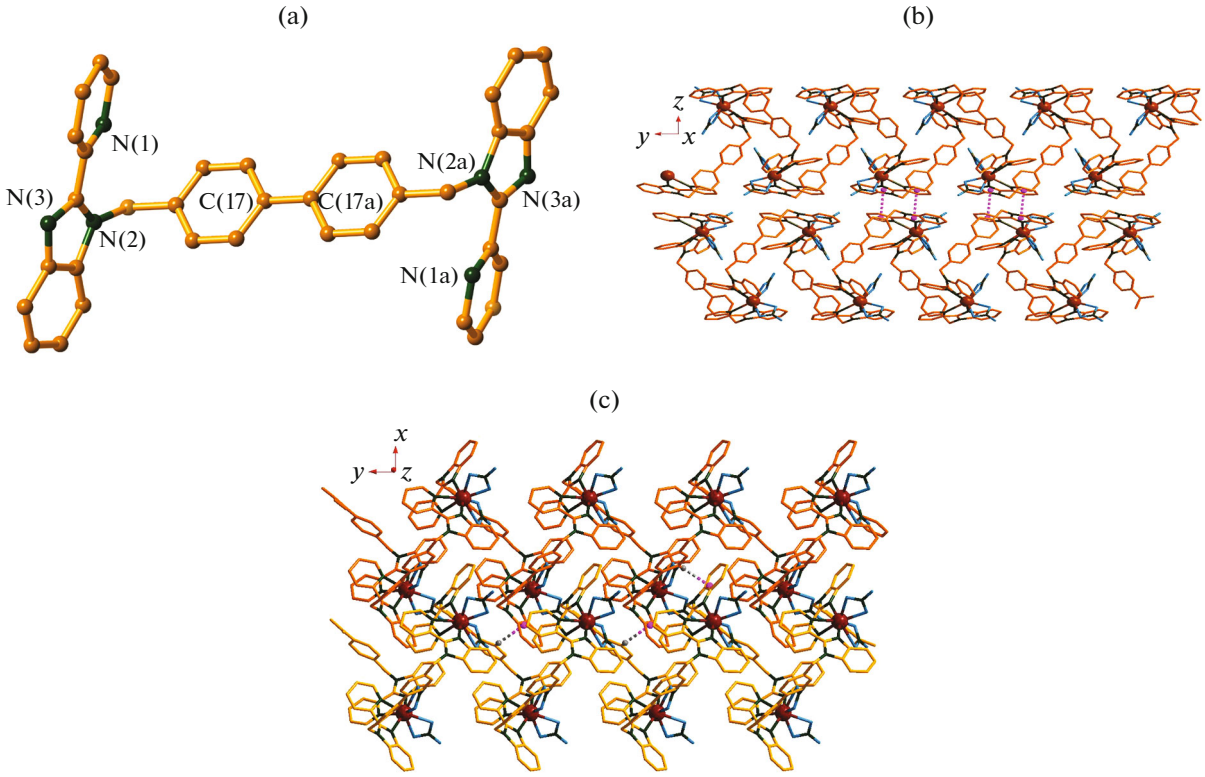

Fig. 3. The crystal structure of organic linker Bpbib in *trans* manner (a); the helical chain extend in *z* axis depending upon the face to face π···π interactions (b); the helical chain extend in *x* axis based on C–H···π force (c).

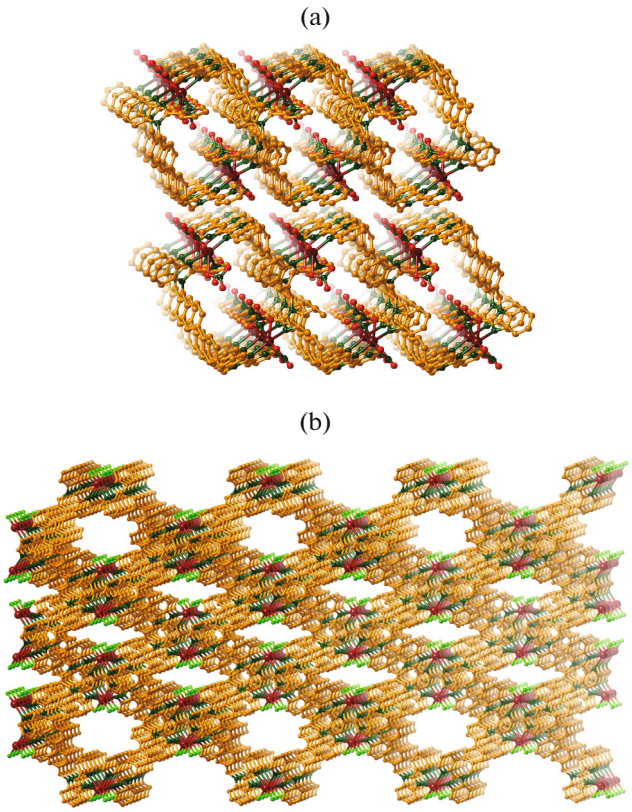

Fig. 4. The crystal packing of complexes of **I** (a) and **II** (b), the hydrogen atoms and solvent molecules are omitted for clarity.

π···π interactons, the adjacent hydrogen bonds further stabilized the crystal packing, which lead to the formation of a 3D architecture (Fig. 4a).

Owing to the size and shape variation of anion, chloride was used instead of nitrate to aid crystallization of complex **II** with structural diversity. The asymmetric unit is composed of one Cd(II) center, half a Bpbib connector, one bound chloride anion and one methanol molecule. The distorted octahedral Cd(II) coordination sphere is defined by three nitrogen atoms and one chloride anion to complete the equatorial plane, whereas the apical positions are occupied by one chloride anion together with one pyridyl nitrogen atom (Fig. 1b). To balance the charge of metal center, the chloride anion may stem from the thermolysis of chloroform and serves in terminal fashion. The Cd(II) center was connected by *trans* bridging Bpbib, the alternate connectivity generating a zigzag coordination pattern. The Bpbib possesses C_i symmetry, in which dihedral angle of pyridyl ring and benzimidazole moiety is 27.19°. The corresponding angle and twist angles around methylene are 113.122° and 31.835°, respectively. In **I** and **II**, the variations of angle and twist angles assisted the flexibility and conformation manner diversity, which are aroused by anion effect. Each Bpbib is coordinated to two separate Cd(II) centers, whilst the adjacent Cd···Cd separation is 18.919 Å.

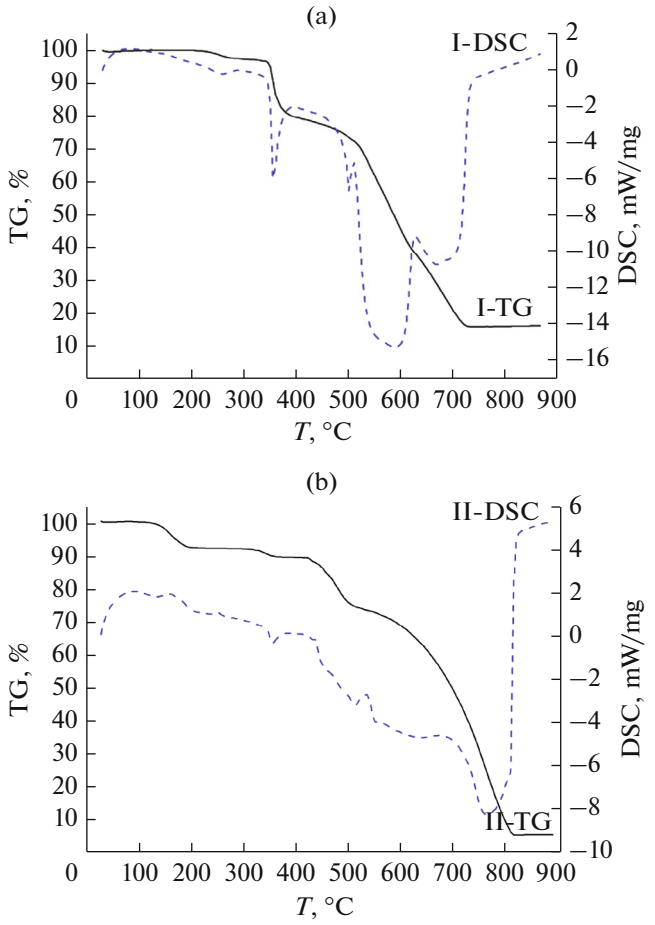

Fig. 5. The plots of TG and DSC analyses of complexes **I** (a) and **II** (b).

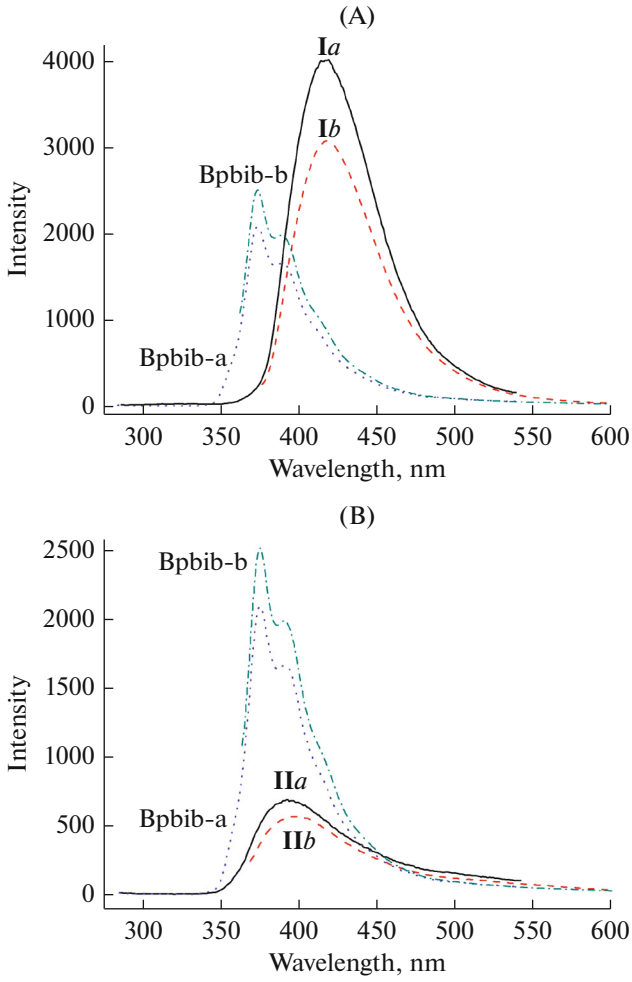

Fig. 6. Emission spectra of the organic linker of Bpbib (λ_{em} = 375 nm) excited at 275, 353 nm (*a*, *b*) and complexes: A—**I** (λ_{em} = 417 nm) excited at 277, 367 nm (*a*, *b*) and B—**II** (λ_{em} = 392 nm) excited at 275, 358 nm (*a*, *b*), respectively.

On the basis of the above discussion, the anion effect, deriving from the subtly balanced metal size, electronic configuration and organic linker conformation, exerts profound influence over coordination assembly process by fine-tuning of metal coordination geometry. Multiple hydrogen bonding interactions was also observed in the crystal lattice of **II**. The C···Cl distances are 3.646(8) Å for C(9)–H(9)···Cl(1), 3.609(6) for C(18)–H(18)···Cl(1), and the C···O distance is 3.513(10) for C(13)–H(13*B*)···O(1). The H···Cg separation is 2.75 Å for H(3)···Cg(5) (ring of C(7)···C(12)) [26, 27]. These secondary interactions extended the infinite 1D pattern into 3D supramolecular architectures (Fig. 4b).

The air-stable complexes **I** and **II** can retain their crystalline integrity at ambient temperature, and their thermal stabilities were also explored by thermogravimetric (TG) and differential scanning calorimetric (DSC) analysis, as illustrated in Fig. 5. Complex **I** shows initial mass loss of 2.13% attained 280°C, assigned to the loss of corresponding solvent molecules (calcd. 1.95%). Complex **II** exhibits initial mass loss of 7.92% until 205°C, attributed to the leave of corresponding solvent molecules (calcd. 7.84%).

The emission spectral behaviors of organic linker Bpbib and as-synthesized complexes **I** and **II** have been studied at room temperature. Bpbib has two excited maximum, upon excited at the secondary one at 275 nm and the largest one at 353 nm, which gives the emission spectra Bpbib-a and Bpbib-b with λ_{max} equaling to 375 nm, respectively. Also, both **I** and **II** exhibit two excited maximum. Complex **I**, upon excited at first maximum 277 nm, gives rise to a strong emission band with λ_{max} = 417 nm. Whereas excited at secondary maximum 367 nm, complex I results in a slightly weaker emission band with λ_{max} = 417 nm as well (Fig. 6A). Complex **II** shows weak emission band with λ_{max} = 392 nm upon excitation at the first maximum 275 nm, while excited at the secondary maximum 358 nm, II also yields a slightly weaker emission

with λ_{max} = 392 nm (Fig. 6B). Apparently, the fluorescent behaviors are quite similar to that found for Bpbib, which illustrates the emission peaks may be tentatively assigned to the intraligand transition, and the slight red-shift together with the intensity changes with that of the free ligand may be dominated by the conjunction effects of anion and metal–ligand coordination interactions. Besides, previously reports have also proven the anion nature can arouse structural and behavioral variation [28–30].

ACKNOWLEDGMENTS

We gratefully acknowledge the financial support by He'nan key science and technology research (132102310121), the training and funding Program for young key teacher of Henan University of Urban Construction, and the funding program for young key teacher of He'nan colleges and universities (no. 2013GGJS-175).

REFERENCES

1. Le, T., Epa, V.C., Burden, F.R., and Winkler, D.A., *Chem. Rev.*, 2012, vol. 112, p. 2889.
2. Artizzu, F., Mercuri, M.L., Serpe, A., and Deplano, P., *Coord. Chem. Rev.*, 2011, vol. 257, p. 2514.
3. Barone, G., Terenzi, A., Lauria, A., et al., *Coord. Chem. Rev.*, 2013, vol. 257, p. 2848.
4. Sun, Y.-G., Ji, S.-F., Huo, P., et al., *Inorg. Chem.*, 2014, vol. 53, p. 3078.
5. Potapov, A.S., Nudnova, E.A., Khlebnikov, A.I., et al., *Inorg. Chem. Commun.*, 2015, vol. 53, p. 72.
6. Sun, S., Liu, L.-J., Ma, W.-Y., et al., *J. Solid State Chem.*, 2015, vol. 225, p. 1.
7. Hu, J., Yao, H., Bai, Y., et al., *Polyhedron*, 2014, vol. 78, p. 1.
8. Wang, F.-F., Guo, W., Jiang, C.-H., and Guo, Y.-M., *J. Mol. Struct.*, 2013, vol. 1046, p. 9.
9. Kundu, N., Audhya, A., Abtab, S.M.T., et al., *Cryst. Growth Des.*, 2010, vol. 10, p. 1269.
10. Chen, K., Strasser, C.E., Schmitt, J.C., et al., *Inorg. Chem.*, 2012, vol. 51, p. 1207.
11. Li, Y.-W., Ma, H., Chen, Y.-Q., et al., *Cryst. Growth Des.*, 2012, vol. 12, p. 189.
12. Hu, J., Liao, C., Chen, S., et al., *Inorg. Chem. Commun.*, 2014, vol. 43, p. 126.
13. Lee, H.-H., Park, I.-H., and Lee, S.S., *Inorg. Chem.*, 2014, vol. 53, p. 4763.
14. Lee, S.J., Jung, J.H., Seo, J., et al., *Org. Lett.*, 2006, vol.8, p. 1641.
15. Lee, H. and Lee, S.S., *Org. Lett.*, 2009, vol. 11, p. 1393.
16. Li, X., Gong, Y., Zhao, H., and Wang, R., *Inorg. Chem.*, 2014, vol. 53, p. 12127.
17. Guo, W., Jiang, C.-H., and Guo, Y.-M., *Inorg. Chim. Acta*, 2013, vol. 405, p. 128.
18. Addison, A.W. and Burke, P.J., *J. Heterocycl. Chem.*, 1981, vol. 18, p. 803.
19. Sheldrick, G.M., *SHELXTL-97, Program for Crystal Structure Refinement*, Göttingen (Germany): Univ. of Göttingen, 1997.
20. Sheldrick, G.M., *SHELXS-97, Program for Crystal Structure Solution*, Göttingen (Germany): Univ. of Göttingen, 1997.
21. Sheldrick, G.M., *Acta Crystallogr., Sect A: Found Crystallogr.*, 2008, vol. 64, p. 112.
22. Dolomanov, O.V., Bourhis, L.J., Gildea, R.J., et al., *J. Appl. Cryst.*, 2009, vol. 42, p. 339.
23. Kundu, N., Abtab, S.M.T., Kundu, S., et al., *Inorg. Chem.*, 2012, vol. 51, p. 2652.
24. Mao, J.-G. and Wang, Z., and Clearfield, A., *Inorg. Chem.*, 2002, vol. 41, p. 3713.
25. Dey, S., Mukherjee, T., Sarkar, S., et al., *Transition Met. Chem.*, 2011, vol. 36, p. 631.
26. Venkataramanan, B., Saifudin, M.-A., Jagadese, J.V., and Suresh, V., *CrystEngComm*, 2004, vol. 6, p. 284.
27. Kong, L.-Y., Zhu, H.-F., Huang, Y.-Q., et al., *Inorg. Chem.*, 2006, vol. 45, p. 8098.
28. Li, X., Gong, Y., Zhao, H., and Wang, R., *Inorg. Chem.*, 2014, vol. 53, p. 12127.
29. Konar, S., Jana, A., Das, K., et al., *Inorg. Chim. Acta*, 2013, vol. 395, p. 1.
30. Wang, X.-L., Zhao, W., Hou, J.-L., et al., *Transition Met. Chem.*, 2013, vol. 38, p. 827.